Machine learning forecasts of the cosmic distance duality relation with strongly lensed gravitational wave events

Rubén Arjona,[1,*] Hai-Nan Lin,[2,†] Savvas Nesseris,[1,‡] and Li Tang[3,2,§]

[1] *Instituto de Física Teórica UAM-CSIC, Universidad Autonóma de Madrid, Cantoblanco, 28049 Madrid, Spain*
[2] *Department of Physics, Chongqing University, Chongqing 401331, China*
[3] *Department of Math and Physics, Mianyang Normal University, Mianyang 621000, China*

(Dated: November 6, 2020)

We use simulated data from strongly lensed gravitational wave events from the Einstein Telescope to forecast constraints on the cosmic distance duality relation, also known as the Etherington relation, which relates the luminosity and angular diameter distances $d_L(z)$ and $d_A(z)$ respectively. In particular, we present a methodology to make robust mocks for the duality parameter $\eta(z) \equiv \frac{d_L(z)}{(1+z)^2 d_A(z)}$ and then we use Genetic Algorithms and Gaussian Processes, two stochastic minimization and symbolic regression subclasses of machine learning methods, to perform model independent forecasts of $\eta(z)$. We find that both machine learning approaches are capable of correctly recovering the underlying fiducial model and provide percent-level constraints at intermediate redshifts when applied to future Einstein Telescope data.

I. INTRODUCTION

The first detection of gravitational waves (GWs) by the LIGO/Virgo collaboration was not just limited to the discovery of new astrophysical objects, but it was also instrumental in furthering our understanding of the fundamental properties of gravity and cosmology, by providing tests of gravity in the strong field regime. These observations from black hole and neutron star mergers have, figuratively speaking, shone a light on the population of compact objects in the Universe and the mechanism by which they are formed [1], given some of the most rigorous direct tests to date of General Relativity (GR) [2, 3] and provided the first measurement of a cosmological parameter, the Hubble constant H_0, using GW sources [4].

Moreover, the observation of the binary neutron star merger GW170817 availed us of the opportunity to test gravity both in the strong regime and at large scales, as it was followed by the nearly simultaneous detection of its optical counterpart and allowed us to strongly constrain the GW propagation speed to $|c_g - c| \lesssim \mathcal{O}\left(10^{-15}\right)$ [5], thus challenging a wide range of modified gravity scenarios which are candidates to explain the current acceleration of the Universe [6–11]. The impact of GW observations will be further extended by third generation ground based detectors like the Einstein Telescope (ET) [12] and the space-based interferometer LISA [13].

Similarly to photons, GWs can be gravitationally lensed by the presence of galaxies and clusters of galaxies, producing a deflection in their trajectories, thus generating multiple detection events. This phenomenon is quite intriguing because the clustered matter that lies in between the GW source and the observer can enhance the observed signal [14]. This in turn can cause the luminosity distance to the source and therefore its redshift, if combined with the Hubble parameter H_0 constraints [15], to be underestimated. Sequentially, this would lead to an overestimation of the chirp mass [16].

With the upgraded sensitivity of the third generation of GW detectors, such as the Einstein Telescope (ET), the detection sensitivity of the GW events would be accordingly improved. Thus, with the sufficiently large number of detectable events foreseen [17, 18], it is expected that some of these events could be gravitationally lensed, thus allowing the creation of a considerably large catalogue of strongly lensed GWs event within a few years of operation. For an extensive analysis on how GW lensing is enriched with concrete signatures and features and can be used to search for deviations of GR see Ref. [19].

One of the advantages of strongly lensed GW events comes from their ability to provide simultaneous measurements of both the luminosity and angular diameter distance, i.e $d_L(z)$ and $d_A(z)$ respectively, which in turn could be used to probe fundamental properties of the standard cosmological model. One such example of a possible probe is the cosmic distance duality relation (DDR), also known as the Etherington relation, which relates the luminosity distance to the angular diameter distance [20] via

$$d_L(z) = (1+z)^2 d_A(z), \tag{1}$$

which is valid for any metric theory of gravity like GR and under the condition that the number of gravitons or photons, depending in which context it is applied, is conserved and that they travel along null geodesics in a pseudo-Riemannian spacetime [21]. At this point we can introduce the duality parameter

$$\eta(z) \equiv \frac{d_L(z)}{(1+z)^2 d_A(z)}, \tag{2}$$

* ruben.arjona@uam.es
† linhn@cqu.edu.cn
‡ savvas.nesseris@csic.es
§ tang@cqu.edu.cn

where $\eta(z)$ is a function that accounts for possible deviations from unity and is equal to unity when the DDR holds.

Hence, any violation of the DDR relation at any redshift, i.e $\eta(z) \neq 1$, would be a hint of new physics, which in the case of photons could be caused by different mechanisms, such as the annihilation of photons by the intergalactic dust [22], the coupling of photons with other particles like axions [23] and the variation of fundamental constants [24]. In fact several works have been devoted to test the DDR relation [21, 25–34]. In this paper we show how to reconstruct the DDR relation using mock datasets of strongly lensed GWs.

The use of strongly lensed GW events to measure both angular diameter and luminosity distance is complementary to the approach of Ref. [35], where $\eta(z)$ was constrained using LSST-like mocks of strongly lensed type Ia supernovae (SNIa). Both methods have the advantage of allowing for measurements of the duality parameter without relying on multiple datasets, hence it is competitive with other more traditional tests of the DDR relation where the latter is constrained through the combination of SNIa and BAO observations, as for example it has been forecast in surveys like Euclid [33].

In Ref. [36] the authors proposed a novel method to test the cosmic distance duality relation using the strongly lensed GWs from the Einstein Telescope and in Ref. [37] mock data was generated for this ground-based detector, while a parameterized approach was used to constrain the DDR relation. Here we present a broader analysis by presenting a slightly different methodology which allows us to directly make robust $\eta(z)$ mocks, based on the mocks of d_L and d_A and then we use Genetic Algorithms (GA) and Gaussian Processes (GP), two non-parametric and symbolic regression subclasses of machine learning methods, to reconstruct $\eta(z)$ directly without any underlying model.

The paper is organized as follows: In Sec. II we describe the methodology to generate the ET mock data and the ML implementation. In Sec. III we present our reconstructions for the GP and GA, while in Sec. IV we summarize our conclusions.

II. METHODOLOGY

A. Distance measurements from strongly lensed GW events

1. *Measure d_A from strong lensing*

Here we will now consider the case when a GW emission is strongly lensed by a foreground galaxy, whose mass profile can be modeled by the singular isothermal sphere (SIS) model. We will assume however that GWs propagate following geometric optics, i.e. we neglect wave effects, see Ref. [38] for more details. With this setup then we assume the two images will appear at angular positions θ_1 and θ_2 with respect to the lensing galaxy. Thus, the Einstein radius $\theta_E = |\theta_1 - \theta_2|/2$ will be given by [39]

$$\theta_E = \frac{4\pi\sigma^2_{\rm SIS} d_A(z_l, z_s)}{c^2 d_A(z_s)}, \tag{3}$$

where the velocity dispersion of the lens galaxy is given by $\sigma_{\rm SIS}$, the angular diameter distances from the observer to the source and from the lens to the source are given by $d_A(z_s)$ and $d_A(z_l, z_s)$ respectively. We can invert equation (3) to obtain the distance ratio, which will be given by

$$R_A \equiv \frac{d_A(z_l, z_s)}{d_A(z_s)} = \frac{c^2\theta_E}{4\pi\sigma^2_{\rm SIS}}. \tag{4}$$

If the angular positions and the velocity dispersion are well measured, which would require a precise localization of the GW sources that should be achievable with a network of interferometers, then we can obtain the distance ratio R_A from Eq. (4).

As the two images propagating along different paths will take different amounts of time to reach Earth, then the time delay between the images will be given by [39]

$$\Delta t = \frac{(1+z_l)}{c}\frac{d_A(z_l)d_A(z_s)}{d_A(z_l, z_s)}\Delta\phi, \tag{5}$$

where

$$\Delta\phi = \frac{(\theta_1 - \beta)^2}{2} - \Psi(\theta_1) - \frac{(\theta_2 - \beta)^2}{2} + \Psi(\theta_2), \tag{6}$$

is the Fermat potential difference between two paths and $\Psi(\theta)$ is the rescaled projected gravitational potential of the lens galaxy. By inverting equation (5) we can thus obtain the time-delay distance

$$D_{\Delta t} \equiv \frac{d_A(z_l)d_A(z_s)}{d_A(z_l, z_s)} = \frac{c}{1+z_l}\frac{\Delta t}{\Delta\phi}. \tag{7}$$

If the gravitational potential of the lens galaxy can be measured from photometric and spectroscopic observations, and if the time delay between two images can be well measured, we can obtain the time-delay distance $D_{\Delta t}$ according to Eq. (7).

In a spatially flat universe, the angular diameter distance from lens to source, $d_A(z_l, z_s)$, can be expressed in terms of $d_A(z_s)$ and $d_A(z_l)$ as

$$d_A(z_l, z_s) = d_A(z_s) - \frac{1+z_l}{1+z_s} d_A(z_l). \tag{8}$$

Equation (8), together with equations (4) and (7) allow us to uniquely solve for $d_A(z_s)$, which reads

$$d_A(z_s) = \frac{1+z_l}{1+z_s}\frac{R_A D_{\Delta t}}{1-R_A}, \tag{9}$$

where R_A and $D_{\Delta t}$ are given by equations (4) and (7), respectively. The error on $d_A(z_s)$ propagates from the errors on R_A and $D_{\Delta t}$, i.e.,

$$\frac{\delta d_A(z_s)}{d_A(z_s)} = \sqrt{\left(\frac{\delta R_A}{R_A(1-R_A)}\right)^2 + \left(\frac{\delta D_{\Delta t}}{D_{\Delta t}}\right)^2}, \quad (10)$$

where

$$\frac{\delta R_A}{R_A} = \sqrt{\left(\frac{\delta\theta_E}{\theta_E}\right)^2 + 4\left(\frac{\delta\sigma_{\rm SIS}}{\sigma_{\rm SIS}}\right)^2}, \quad (11)$$

and

$$\frac{\delta D_{\Delta t}}{D_{\Delta t}} = \sqrt{\left(\frac{\delta\Delta t}{\Delta t}\right)^2 + \left(\frac{\delta\Delta\phi}{\Delta\phi}\right)^2}. \quad (12)$$

Having the observables (z_l, z_s, Δt, $\Delta\phi$, θ_E, $\sigma_{\rm SIS}$) measured, then $d_A(z_s)$ and its uncertainty can be obtained from Eqs. (9)–(12).

2. *Measure d_L from GW signals*

We now consider an unlensed GW source. In this case the luminosity distance to the source can be directly obtained by matching the GW signals to the GW templates. GW detectors based on the interferometers such as ET measure the change of difference of two optical paths caused by the pass of GW signals. In general, the response of a GW detector on GW signals will depend on the spacetime strain, which is the linear combination of the two polarization states $h_+(t)$ and $h_\times(t)$

$$h(t) = F_+(\theta,\varphi,\psi)h_+(t) + F_\times(\theta,\varphi,\psi)h_\times(t), \quad (13)$$

where the beam-pattern functions $F_+(\theta,\varphi,\psi)$ and $F_\times(\theta,\varphi,\psi)$ do not only depend on the configuration of the detector, but they also depend on the position of the GW source (θ,φ) and the polarization angle ψ. For example, in the case of the ET, the beam-pattern functions can be found in Ref. [40].

In the post-Newtonian and stationary phase approximation, the strain $h(t)$ can be written in the the Fourier space by [40, 41]

$$\mathcal{H}(f) = \mathcal{A}f^{-7/6}\exp[i(2\pi f t_0 - \pi/4 + 2\psi(f/2) - \varphi_{(2,0)})], \quad (14)$$

where the Fourier amplitude is given by

$$\mathcal{A} = \frac{1}{d_L}\sqrt{F_+^2(1+\cos^2\iota)^2 + 4F_\times^2\cos^2\iota} \times\sqrt{\frac{5\pi}{96}}\pi^{-7/6}\mathcal{M}_c^{5/6}, \quad (15)$$

where ι is the inclination angle, d_L is the luminosity distance, $\mathcal{M}_c = M\eta^{3/5}$ is the chirp mass, $M = m_1 + m_2$ is the total mass, $\eta = m_1m_2/M^2$ is the symmetric mass ratio and m_1 and m_2 are the component masses of the binary in the comoving frame. In the case of a GW source at redshift z, $\mathcal{M}_c$ in equation (15) should be interpreted as the chirp mass in the observer frame, which can be related to that of the comoving frame via $\mathcal{M}_{c,\rm obs} = (1+z)\mathcal{M}_{c,\rm com}$. Finally, it should be noted that the exponential term on the right-hand-side of Eq. (14) is just a phase term, which is unimportant in our analysis.

The signal-to-noise ratio (SNR) of the detector's response to a GW signal is given by [41]

$$\rho_i = \sqrt{\langle\mathcal{H},\mathcal{H}\rangle}, \quad (16)$$

where the inner product may be defined as

$$\langle a,b\rangle = 4\int_{f_{\rm lower}}^{f_{\rm upper}}\frac{\tilde{a}(f)\tilde{b}^*(f) + \tilde{a}^*(f)\tilde{b}(f)}{2}\frac{df}{S_h(f)}, \quad (17)$$

and in the latter equation, $\tilde{a}$ and a^* stand for the Fourier transformation and complex conjugation of a, respectively, while $S_h(f)$ is the one-side noise power spectral density (PSD) of ET, $f_{\rm lower} = 1$ and $f_{\rm upper} = 2f_{\rm LSO}$ are the lower and upper cutoffs of the frequency, $f_{\rm LSO} = 1/(6^{3/2}2\pi M_{\rm obs})$ is the orbit frequency at the last stable orbit, $M_{\rm obs} = (1+z)(m_1+m_2)$ is the total mass in the observer frame. Finally, the PSD for ET is given by [42]

$$S_h(f) = 10^{-50}(2.39\times10^{-27}x^{-15.64} + 0.349x^{-2.145} + 1.76x^{-0.12} + 0.409x^{1.1})^2\ {\rm Hz}^{-1}. \quad (18)$$

For the ET, three arms interfere with each other in pairs, hence the combined SNR is given by

$$\rho = \left[\sum_{i=1}^{3}\rho_i^2\right]^{1/2}. \quad (19)$$

In general, there is degeneracy between the luminosity distance d_L and inclination angle ι, so the uncertainty on d_L may be large. However, if the GW event is accompanied by a short gamma-ray burst (GRB), we can assume that the inclination angle is small, since GRB is expected to be produced in a narrow beam. In this case the degeneracy between d_L and ι breaks, and the uncertainty on d_L can be estimated as

$$\delta d_L = \sqrt{\left(\frac{2d_L}{\rho}\right)^2 + (0.05zd_L)^2}, \quad (20)$$

where the $0.05z$ term represents the uncertainty arising from weak lensing effect caused by the intergalactic medium along the line-of-sight.

The above discussion is applicable for unlensed GW events. However, the situation is subtle for strongly lensed GW events. Due to the magnification effect of lensing, the luminosity distance measured from the strongly lensed GW signals is not the true distance. Since the amplitude of GW signal $\mathcal{A}$ is magnified by the lensing effect by a factor of $\sqrt{\mu_\pm}$ [43], and the luminosity distance d_L is inversely proportional to $\mathcal{A}$, the true luminosity distance should be $d_L^{\rm true} = \sqrt{\mu_\pm}d_L^{\rm obs}$. If the magnification

factor $\sqrt{\mu_\pm}$ can be independently measured through photometric observations, we can obtain the true distance $d_L^{\rm true}$. The uncertainty of $\mu_\pm$ will also propagate to d_L. Therefore, the total uncertainty on $d_L(z_s)$ is given by

$$\frac{\delta d_L^{\rm total}}{d_L} = \sqrt{\left(\frac{2}{\rho}\right)^2 + (0.05 z_s)^2 + \frac{1}{4}\left(\frac{\delta\mu_\pm}{\mu_\pm}\right)^2}. \quad (21)$$

B. The mock DDR data

In order to forecast direct measurements of the duality parameter $\eta(z)$ from the ET, we use mock distance data based on individual measurements of the luminosity and angular diameter distances $d_L(z)$ and $d_A(z)$ respectively, as described previously. To join the two measurements and derive the $\eta(z)$ data, we follow the pioneering work of Ref. [35] using an MCMC-like approach to create mock samples.

In an nutshell we can summarize this approach as follows. First, we assume a fiducial cosmology based on the flat ΛCDM model with parameters $H_0 = 70$ km s^{-1} Mpc^{-1}, $\Omega_{m,0} = 0.3$ and $\Omega_k = 0$. Then, based on the redshift distribution of sources, either Neutron star-Neutron star (NS-NS) or Neutron star-Black Hole (NS-BH), we calculate at every point in redshift the corresponding angular diameter distance $d_A(z)$ and the luminosity distance $d_L(z)$ via the methodology of Ref. [37] as described earlier. At this point, we also introduce a modification of the luminosity distance so that the observed luminosity distance would be proportional to the "bare" one as:

$$d_{L,\rm obs}(z) = (1+z)^{\epsilon(z)} d_{L,\rm bare}(z), \quad (22)$$

such that it corresponds to a duality parameter $\eta(z) = (1+z)^{\epsilon(z)}$, which should be equal to unity if no deviations are present, i.e. $\epsilon(z) \to 0$ in the ΛCDM model and $\eta(z) = 1$. In particular, we assume that to lowest order, any deviations are small enough that we can assume a constant $\epsilon(z) = \epsilon_0$. In general, any such deviations on the GW sector could be due to modifications of gravity, see for example Ref. [34]. Specifically, in what follows we will assume four specific scenarios: the vanilla ΛCDM case for $\epsilon_0 = 0$ and three more cases with one mild and two stronger deviations of the duality relation with $\epsilon_0 = 0.01,\ 0.05,\ 0.1$.

After we have calculated the fiducial values of the cosmological distances, we can then make mock samples of the duality parameter $\eta(z)$ directly via the following procedure: First, at each redshift we create mock distances $d_A(z_s)$ and $d_L(z_s)$ based on a Gaussian distribution using the fiducial values and 1σ errors based on the methodology of Ref. [37], such that for the mock we have

$$(D_{i,\rm mock}, \sigma_{i,\rm mock}) \to \mathcal{N}(D_{i,\rm fid}, \sigma_{i,\rm fid}), \quad (23)$$

where $i = 1 \dots N_{\rm lens}$, D_i representing either d_A or d_L, while $\sigma_{i,\rm fid}$ are the errors. Then, to make a mock sample of $\eta(z_i)$ values we can use Eq. (2) and an MCMC-like approach to obtain the mean values and the errors of the data as follows:

1. Using the mock distances at each redshift $D_{i,\rm mock}$ we draw 10,000 random samples from the assumed distribution for $D_{i,\rm mock}$.

2. We then estimate $\eta(z_i)$ at each redshift z_i for each of the 10,000 random points using Eq. (2) to obtain 10,000 realisations of the distribution of $\eta(z_i)$.

3. Finally, we estimate the mean and standard deviation of $\log_{10}\eta(z_i)$ at each redshift point to create our final mock sample.

The main advantage of this MCMC-like approach is that it does not depend on error propagation for the various quantities, which could be highly non-trivial for complicated modified gravity models, but it also preserves the statistical properties of the samples. In Ref. [34] it was shown that this approach allows for the creation of mocks that have minimal external biases, theoretical, statistical or otherwise.

Finally, we should note that we chose to make mocks of $\log_{10}\eta(z_i)$ instead of simply $\eta(z_i)$, as we found that the distribution of the latter is somewhat non-gaussian, while on the other hand, $\log_{10}\eta(z_i)$ is very close to being normally distributed around zero, i.e. $\log_{10}\eta(z_i) \sim \mathcal{N}(0, \sigma_{\log_{10}\eta(z_i)})$. Then, having created the $\log_{10}\eta(z_i)$ samples, we consider a likelihood of the form [35]:

$$-2\ln\mathcal{L} = \sum_{i=1}^{N_{\rm lens}} \left(\frac{\log_{10}\eta(z_i) - \log_{10}\eta^{\rm th}(z_i)}{\sigma_{\log_{10}\eta(z_i)}}\right)^2 \quad (24)$$

where $\eta^{\rm th}(z_i)$ is the theoretical value of $\eta(z_i)$. In our actual analysis we will consider the somewhat optimistic case of $N_{\rm lens} = 100$ as an example that illustrates our approach.

C. Machine learning

Machine learning (ML) is a subset of artificial intelligence designed to model a given set of data. ML approaches have been proven to be successful at processing and extracting essential information from large amounts of data and can get rid of the problem of model bias [44], while also being very effective in testing the consistency of the dataset model independently and also for searching tensions or systematics. In what follows we will describe two particular classes of ML methods, the Genetic Algorithms (GA) and the Gaussian Processes (GP).

1. The Genetic Algorithms

Here we introduce the theoretical background of the implementation of the GA in our analysis. For a more in-depth discussion on the GA and several applications to

cosmology see Refs. [32, 45–51]. The GA have been also applied in a wide range of areas such as particle physics [52–54], astronomy and astrophysics [55–57] and other fields like computational science, economics, medicine and engineering [58, 59]. For other symbolic regression methods applied in physics and cosmology see [60–67].

The GA are a particular class of ML methods mostly developed to perform unsupervised regression of data, which implies that the GA can be used for non-parametric reconstructions finding an analytic function that describes the data, using one or more variables. This is achieved by mimicking the notion of biological evolution via the concept of natural selection, as conveyed by the genetic operations of mutation and crossover. In essence, a set of test functions evolves over time through the effect of the stochastic operators of crossover, i.e the joining of two or more individuals to form an offspring, and mutation, i.e a random alteration of an individual. This process is consequently repeated thousands of times so as to ensure convergence, while different random seeds can be tested to further explore the functional space.

Since by construction the GA is a stochastic approach, the probability that a set or a population of functions will produce offspring is normally assumed to be proportional to its fitness to the data, which in our analysis is a χ^2 statistic and indicates how good every individual agrees with the data. In this analysis we reconstruct the DDR parameter $\log_{10}\eta(z_i)$ directly from the data, and the procedure to its reconstruction proceeded as follows. First, our predefined grammar consisted on the following orthogonal basis of functions: exp, log and polynomials and a set of operations $+, -, \times, \div$.

We also imposed a prior motivated by physical reasons. The only assumption made is that $\eta(z)$ is equal to 1 at out present time $z = 0$. This is natural to expect since mechanisms where the DDR is violated are cumulative, as photons interact with interceding constituents along the line of sight. Hence, such an event does not have time to occur at vanishing redshifts. This can also be seen by taking the limit for $z = 0$ at Eq. (2) and assuming the Hubble law, i.e. $\lim_{z\to 0}\eta(z) = 1$. Finally, we make no assumptions on the curvature of the Universe or any modified gravity or dark energy model.

We also required that all functions reconstructed by the GA are continuous and differentiable, without any singularities in the redshift probed by the data, avoiding in this manner overfitting or any spurious reconstructions. We emphasize that the choice of the grammar and the population size has already been tested in Ref. [45][1]. In the same manner, the seed numbers play also a big role since they are used to create the initial population of functions used later on by the GA.

Once the initial population has been constructed, the fitness of each member is evaluated by a χ^2 statistic, using the $\eta(z)$ data directly as input. Afterwards, using a tournament selection, see Ref. [45] for more details, the best-fitting functions in each generation are chosen and the two stochastic operations (crossover and mutation) are used. In order to assure convergence, the GA process is then repeated thousands of times and with various random seeds, so as to properly explore the functional space. Then the final output of the code is a function of $\eta(z)$ that describes the evolution of the DDR.

Finally, for the statistical interpretation of the data, the errors of the reconstructed functions where estimated through the path integral approach which was originally implemented in Refs. [47, 48] which scans over all possible functions that might be produced by the GA. This error reconstruction method has been exhaustively examined and compared against a bootstrap Monte-Carlo by Ref. [47].

2. The Gaussian Processes

We also use the Gaussian Processes approach in order to provide an alternative to the GA reconstruction and minimize any potential biases due to the reconstruction approach. Traditionally, a Gaussian process (GP) is defined as an ensemble of random variables that have a joint Gaussian distribution [68]. The GP in general is determined by the mean, usually assumed to be zero or some fiducial model, and the covariance. In our case the GP random variables stand for the duality parameter $\log_{10}\eta(z_i)$. On the other hand, the covariance function, also known as a kernel, is denoted by $k(x, \tilde{x})$ and encodes the correlations of the different GP random variables.

Lately the GPs have been used in the reconstruction of a plethora of cosmological data, see e.g. [69–77], while the proper choice of the kernel remains a hotly debated issue in the literature, as it can strongly affect the GP reconstruction. In Ref. [78] it was found that a kernel that works quite well for cosmological data is the so-called Matérn class of kernels, given by [68]:

$$k(x,\tilde{x}) = \sigma_M^2 \frac{2^{1-\nu}}{\Gamma(\nu)} \left(\frac{\sqrt{2\nu}(x-\tilde{x})}{\ell}\right)^{\nu} \times K_\nu\left(\frac{\sqrt{2\nu}(x-\tilde{x})}{\ell}\right), \tag{25}$$

where K_ν is a modified Bessel function, ν determines the shape of the covariance function, which asymptotes to the Gaussian limit as $\nu \to \infty$, while $\Gamma(\nu)$ is the gamma function.

Furthermore, the parameter ℓ describes the length scales over which the function varies, while the parameter σ_M corresponds to the magnitude of these variations. The parameter ν is further chosen to be a half-integer to minimize the dependence on the Bessel function [78]. High values of ν make the GP smoother but for $\nu \geq 7/2$ the results are practically indistinguishable from each other, so we make the choice $\nu = 5/2$. In our analysis we

[1] See for example Fig. 2 of Ref. [45].

use the GP Python package `george` [79] to reconstruct of $\log_{10}\eta(z)$ with the kernel as described above.

Finally, similarly to the GA case described in the previous section, we have also imposed a prior on the GP reconstructions which is motivated by physical reasons. Specifically, we again demand that $\eta(z)$ is equal to unity at out present time $z = 0$, i.e. $\eta(z = 0) = 1$. Again, this is necessary to ensure our reconstructions are physical, while at the same time keeping our analysis general enough.

III. RESULTS

We will now present the results of the reconstruction for both the GA and GP approaches. In particular, in Figs. 1 and 2 we show a particular realization of the $\log_{10}\eta(z_i)$ data mocks for $N_{\rm lens} = 100$, along with the fiducial model (dashed black line), the case of $\log_{10}\eta = 0$ (dashed green line), and the corresponding best-fit (solid colored line) for the GA and the GP for $\epsilon = (0, 0.01, 0.05, 0.10)$ in the top left, top right, bottom left and bottom right panels respectively. The data is shown as grey points in the background and the shaded band corresponds to the 1σ confidence region for the GA (red band) and the GP (magenta band) in the two plots. Note that for the different values of ϵ for the mocks, we keep the same random seed number so that our analysis is not complicated by statistical fluctuations and the interpretation of our results is more straightforward.

The only physical priors used in the reconstruction was the assumption that $\lim_{z\to 0}\eta(z) \to 1$, which follows naturally from the definition of $\eta(z)$ via Eq. (2) and the fact that, at zero redshift the causes of any deviation (for example either axions for light or modified gravity for the GW) have had no time to yet act, which is necessary to ensure that our results are physical.

As can be seen in Figs. 1 and 2, in all cases both the GA and the GP capture the behavior of the data accurately and remain close to the fiducial model, well within the 1σ region. Furthermore, for both ML approaches we find that the reconstructed errors are consistent with each other, thus we are confident in our reconstruction as the GA and the GP are in principle rather different reconstruction methods. In particular, we see in both the GA and GP cases that when $\epsilon = (0.05, 0.10)$ both ML approaches find a clear deviation from the null hypothesis, i.e. $\log_{10}\eta = 0$ (dashed green line) for $0 \leq z \leq 3.5$. For higher redshifts, due to the lack of points the errors of the reconstruction become larger and the statistical significance of the detection diminishes.

IV. CONCLUSIONS

With the advent of GW observations an exciting new window has opened into the Universe. Moreover, a possible detection of strong GW lensing will allow for the testing of fundamental hypotheses of the standard cosmological model as it will provide a test of gravity in the strong field regime, but will also allow for tests of the DDR, similar to that proposed in Ref. [35] for strongly lensed SnIa systems. This exciting possibility was first proposed in Ref. [37], where parametric constraints of the DDR variable $\eta(z)$, given by Eq. (2) were presented.

Here, we extended the work of Ref. [37] in two crucial ways. First, we presented a methodology which allows for the direct creation of $\eta(z)$ data, similar to that of Ref. [35]. We showed an example of this approach using mock ET measurements of d_L and d_A from strongly lensed GW events, which were then combined to create mock $\eta(z)$ data with an MCMC-like approach, as described in Sec. II B. It is important to stress that given the raw measurements of d_L and d_A, the measurements of $\eta(z)$ can be derived without using any dark energy model or beyond the standard model (BSM) theory.

Second, instead of using parametric models for $\eta(z)$, which may carry theoretical bias or miss important features in the data, here we used two specific ML approaches. In particular, we employed the Genetic Algorithms and the Gaussian Processes, which are two non-parametric and symbolic regression subclasses of ML methods, to reconstruct $\eta(z)$ directly without using any underlying model.

Following our methodology, we created a realization of mock $\eta(z)$ data for $\epsilon = (0, 0.01, 0.05, 0.10)$, assuming the ET specifications, and then used the GA and the GP to directly reconstruct $\eta(z)$. The reconstructions are shown in Figs. 1 and 2 where as can be seen, both the GA and the GP capture the behavior of the data accurately and remain close to the fiducial model, well within the 1σ region for all values of the duality parameter ϵ. Furthermore, in the two most extreme cases of $\epsilon = (0.05, 0.10)$ both the GA and the GP find deviations from zero in the redshift range $0 \leq z \leq 3.5$.

We thus find that both machine learning approaches are capable of correctly recovering the underlying fiducial model and providing percent-level constraints at intermediate redshifts, when applied to future Einstein Telescope data, thus opening the door to direct tests of the fundamental principles of the standard cosmological model in the coming decades.

Numerical Analysis Files: The Genetic Algorithm codes used by the authors in the analysis of the paper can be found at https://github.com/snesseris and https://github.com/RubenArjona. For the Gaussian process analysis we use the publicly available python package `george` found at https://github.com/dfm/george.

ACKNOWLEDGEMENTS

The authors thank N. Hogg and F. Renzi for useful discussions and comments on the draft. S. N. and

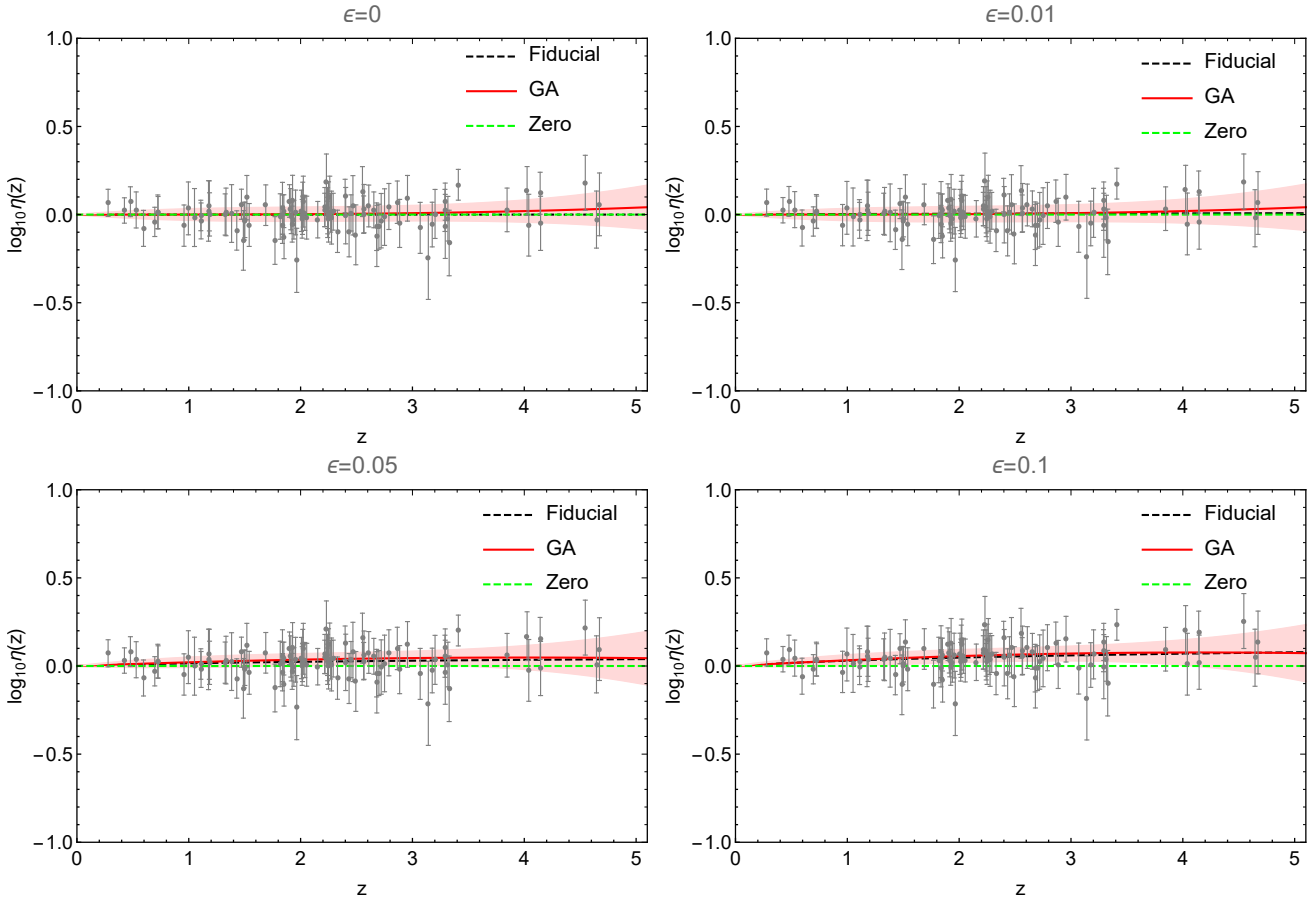

FIG. 1. The $\eta(z)$ data mocks along with the fiducial model (black dashed line), the case of $\log_{10}\eta = 0$ (dashed green line), the corresponding best-fit (solid colored line) for the GA for $\epsilon = (0, 0.01, 0.05, 0.10)$ in the top left, top right, bottom left and bottom right panels respectively. In all cases the $\eta(z)$ data is shown as grey points in the background and the shaded band corresponds to the 1σ confidence region for the GA (red band).

R. A. acknowledge support from the Research Project PGC2018-094773-B-C32 and the Centro de Excelencia Severo Ochoa Program SEV-2016-0597. S. N. also acknowledges support from the Ramón y Cajal program through Grant No. RYC-2014-15843. The work of H.-N. Lin, and L. Tang has been supported by the National Natural Science Fund of China under grant Nos. 11603005, 11775038 and 11947406.

[1] B. Abbott *et al.* (LIGO Scientific, Virgo), Astrophys. J. Lett. **882**, L24 (2019), arXiv:1811.12940 [astro-ph.HE].
[2] B. Abbott *et al.* (LIGO Scientific, Virgo), Phys. Rev. Lett. **123**, 011102 (2019), arXiv:1811.00364 [gr-qc].
[3] B. Abbott *et al.* (LIGO Scientific, Virgo), Phys. Rev. D **100**, 104036 (2019), arXiv:1903.04467 [gr-qc].
[4] B. Abbott *et al.* (LIGO Scientific, Virgo, 1M2H, Dark Energy Camera GW-E, DES, DLT40, Las Cumbres Observatory, VINROUGE, MASTER), Nature **551**, 85 (2017), arXiv:1710.05835 [astro-ph.CO].
[5] B. P. Abbott, R. Abbott, T. Abbott, F. Acernese, K. Ackley, C. Adams, T. Adams, P. Addesso, R. Adhikari, V. Adya, *et al.*, The Astrophysical Journal Letters **848**, L13 (2017).
[6] P. Creminelli and F. Vernizzi, Phys. Rev. Lett. **119**, 251302 (2017), arXiv:1710.05877 [astro-ph.CO].
[7] J. M. Ezquiaga and M. Zumalacárregui, Phys. Rev. Lett. **119**, 251304 (2017), arXiv:1710.05901 [astro-ph.CO].
[8] T. Baker, E. Bellini, P. Ferreira, M. Lagos, J. Noller, and I. Sawicki, Phys. Rev. Lett. **119**, 251301 (2017), arXiv:1710.06394 [astro-ph.CO].
[9] J. Sakstein and B. Jain, Phys. Rev. Lett. **119**, 251303 (2017), arXiv:1710.05893 [astro-ph.CO].
[10] L. Lombriser and A. Taylor, JCAP **03**, 031 (2016), arXiv:1509.08458 [astro-ph.CO].
[11] L. Lombriser and N. A. Lima, Phys. Lett. B **765**, 382 (2017), arXiv:1602.07670 [astro-ph.CO].
[12] M. Maggiore *et al.*, JCAP **03**, 050 (2020), arXiv:1912.02622 [astro-ph.CO].
[13] P. Amaro-Seoane *et al.* (LISA), (2017), arXiv:1702.00786 [astro-ph.IM].

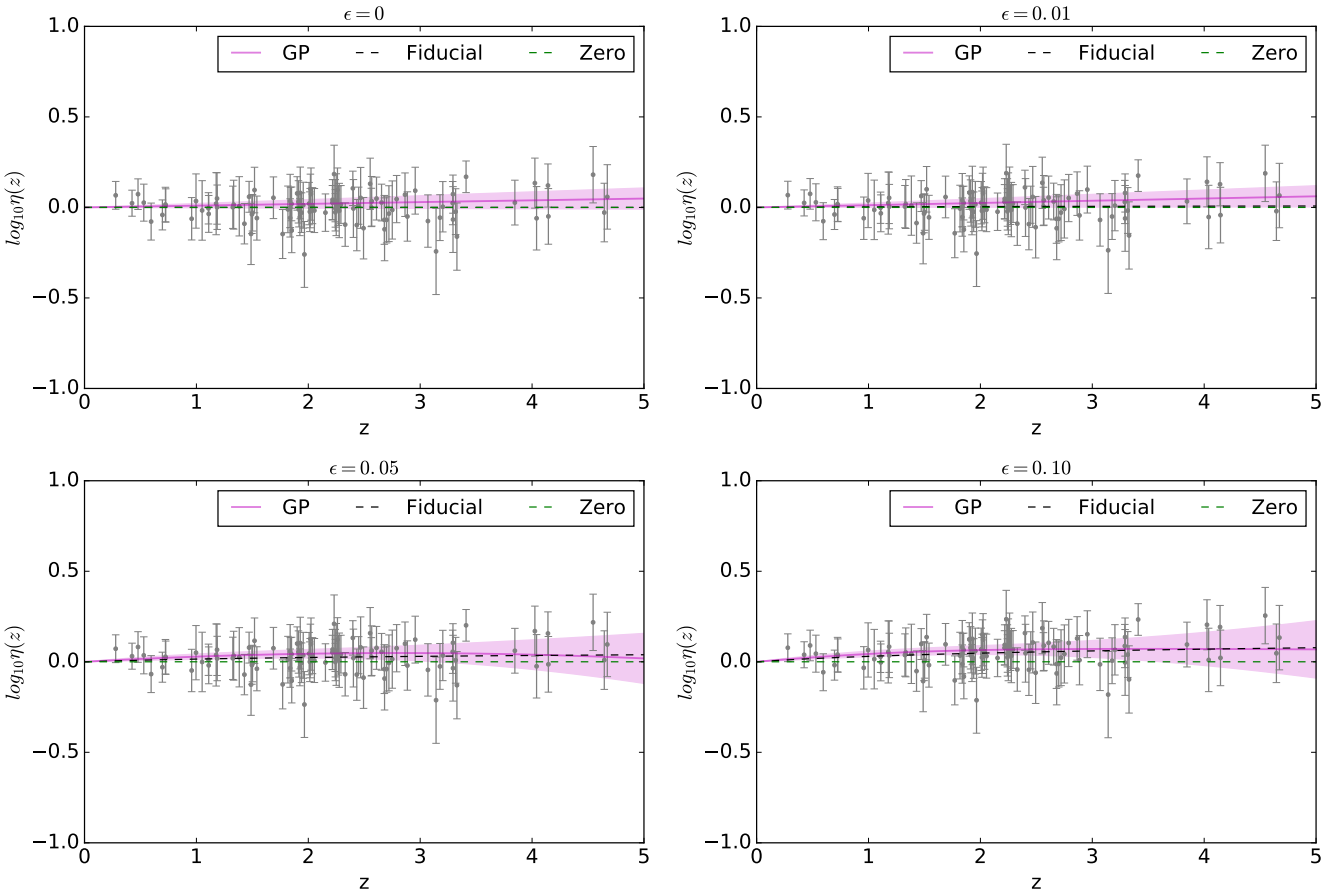

FIG. 2. The $\eta(z)$ data mocks along with the fiducial model (black dashed line), the case of $\log_{10}\eta = 0$ (dashed green line), the corresponding best-fit (solid colored line) for the GP for $\epsilon = (0, 0.01, 0.05, 0.10)$ in the top left, top right, bottom left and bottom right panels respectively. In all cases the $\eta(z)$ data is shown as grey points in the background and the shaded band corresponds to the 1σ confidence region for the GP (magenta band).

[14] G. Cusin, R. Durrer, and I. Dvorkin, (2019), arXiv:1912.11916 [astro-ph.CO].
[15] J. M. Ezquiaga, D. E. Holz, W. Hu, M. Lagos, and R. M. Wald, (2020), arXiv:2008.12814 [gr-qc].
[16] M. Oguri, Mon. Not. Roy. Astron. Soc. **480**, 3842 (2018), arXiv:1807.02584 [astro-ph.CO].
[17] X.-L. Fan, K. Liao, M. Biesiada, A. Piórkowska-Kurpas, and Z.-H. Zhu, Physical Review Letters **118**, 091102 (2017).
[18] K. Liao, X.-L. Fan, X. Ding, M. Biesiada, and Z.-H. Zhu, Nature Communications **8**, 1 (2017).
[19] J. M. Ezquiaga and M. Zumalacárregui, (2020), arXiv:2009.12187 [gr-qc].
[20] I. Etherington, General Relativity and Gravitation **39**, 1055 (2007).
[21] B. A. Bassett and M. Kunz, Phys. Rev. D **69**, 101305 (2004), arXiv:astro-ph/0312443.
[22] P. S. Corasaniti, Mon. Not. Roy. Astron. Soc. **372**, 191 (2006), arXiv:astro-ph/0603833.
[23] P. Tiwari, Phys. Rev. D **95**, 023005 (2017), arXiv:1610.06583 [astro-ph.CO].
[24] G. F. R. Ellis, R. Poltis, J.-P. Uzan, and A. Weltman, Phys. Rev. D **87**, 103530 (2013), arXiv:1301.1312 [astro-ph.CO].
[25] S. Rasanen, J. Valiviita, and V. Kosonen, JCAP **04**, 050 (2016), arXiv:1512.05346 [astro-ph.CO].
[26] R. Lazkoz, S. Nesseris, and L. Perivolaropoulos, JCAP **07**, 012 (2008), arXiv:0712.1232 [astro-ph].
[27] C. Ma and P.-S. Corasaniti, Astrophys. J. **861**, 124 (2018), arXiv:1604.04631 [astro-ph.CO].
[28] V. F. Cardone, S. Spiro, I. Hook, and R. Scaramella, Physical Review D **85**, 123510 (2012).
[29] S. Khedekar and S. Chakraborti, Phys. Rev. Lett. **106**, 221301 (2011), arXiv:1105.1138 [astro-ph.CO].
[30] R. Holanda and V. Busti, Phys. Rev. D **89**, 103517 (2014), arXiv:1402.2161 [astro-ph.CO].
[31] X. Zheng, K. Liao, M. Biesiada, S. Cao, T.-H. Liu, and Z.-H. Zhu, (2020), 10.3847/1538-4357/ab7995, arXiv:2002.09909 [astro-ph.CO].
[32] R. Arjona, JCAP **08**, 009 (2020), arXiv:2002.12700 [astro-ph.CO].
[33] M. Martinelli *et al.* (EUCLID), (2020), arXiv:2007.16153 [astro-ph.CO].
[34] N. B. Hogg, M. Martinelli, and S. Nesseris, (2020), arXiv:2007.14335 [astro-ph.CO].
[35] F. Renzi, N. B. Hogg, M. Martinelli, and S. Nesseris, (2020), arXiv:2010.04155 [astro-ph.CO].

[36] H.-N. Lin and X. Li, Chin. Phys. C **44**, 075101 (2020), arXiv:1911.00263 [gr-qc].

[37] H.-N. Lin, X. Li, and L. Tang, (2020), arXiv:2010.03754 [gr-qc].

[38] R. Takahashi and T. Nakamura, Astrophys. J. **595**, 1039 (2003), arXiv:astro-ph/0305055.

[39] S. Mollerach and E. Roulet, (2002).

[40] W. Zhao, C. Van Den Broeck, D. Baskaran, and T. G. F. Li, Phys. Rev. D **83**, 023005 (2011).

[41] B. Sathyaprakash and B. Schutz, Living Rev. Rel. **12**, 2 (2009), arXiv:0903.0338 [gr-qc].

[42] C. K. Mishra, K. G. Arun, B. R. Iyer, and B. S. Sathyaprakash, Phys. Rev. D **82**, 064010 (2010).

[43] Y. Wang, A. Stebbins, and E. L. Turner, Phys. Rev. Lett. **77**, 2875 (1996).

[44] M. Ntampaka *et al.*, (2019), arXiv:1902.10159 [astro-ph.IM].

[45] C. Bogdanos and S. Nesseris, JCAP **0905**, 006 (2009), arXiv:0903.2805 [astro-ph.CO].

[46] S. Nesseris and A. Shafieloo, Mon. Not. Roy. Astron. Soc. **408**, 1879 (2010), arXiv:1004.0960 [astro-ph.CO].

[47] S. Nesseris and J. Garcia-Bellido, JCAP **1211**, 033 (2012), arXiv:1205.0364 [astro-ph.CO].

[48] S. Nesseris and J. García-Bellido, Phys. Rev. **D88**, 063521 (2013), arXiv:1306.4885 [astro-ph.CO].

[49] D. Sapone, E. Majerotto, and S. Nesseris, Phys. Rev. D **90**, 023012 (2014), arXiv:1402.2236 [astro-ph.CO].

[50] R. Arjona and S. Nesseris, (2020), arXiv:2001.11420 [astro-ph.CO].

[51] R. Arjona and S. Nesseris, Phys. Rev. D **101**, 123525 (2020), arXiv:1910.01529 [astro-ph.CO].

[52] S. Abel, D. G. Cerdeño, and S. Robles, (2018), arXiv:1805.03615 [hep-ph].

[53] B. C. Allanach, D. Grellscheid, and F. Quevedo, JHEP **07**, 069 (2004), arXiv:hep-ph/0406277 [hep-ph].

[54] Y. Akrami, P. Scott, J. Edsjo, J. Conrad, and L. Bergstrom, JHEP **04**, 057 (2010), arXiv:0910.3950 [hep-ph].

[55] M. Wahde and K. Donner, Astronomy & Astrophysics **379**, 115 (2001).

[56] V. Rajpaul, in *Proceedings, 56th Annuall Conference of the South African Institute of Physics (SAIP 2011): Gauteng, South Africa, July 12-15, 2011* (2012) pp. 519–524, arXiv:1202.1643 [astro-ph.IM].

[57] M. Ho, M. M. Rau, M. Ntampaka, A. Farahi, H. Trac, and B. Poczos, (2019), arXiv:1902.05950 [astro-ph.CO].

[58] M. Affenzeller, S. Wagner, S. Winkler, and A. Beham, *Genetic algorithms and genetic programming: modern concepts and practical applications* (Chapman and Hall/CRC, 2009).

[59] S. Sivanandam and S. Deepa, in *Introduction to genetic algorithms* (Springer, 2008) pp. 15–37.

[60] S.-M. Udrescu and M. Tegmark, (2019), arXiv:1905.11481 [physics.comp-ph].

[61] Y. Setyawati, M. Pürrer, and F. Ohme, Class. Quant. Grav. **37**, 075012 (2020), arXiv:1909.10986 [astro-ph.IM].

[62] H. Vaddireddy, A. Rasheed, A. E. Staples, and O. San, arXiv preprint arXiv:1911.05254 (2019).

[63] K. Liao, A. Shafieloo, R. E. Keeley, and E. V. Linder, Astrophys. J. Lett. **886**, L23 (2019), arXiv:1908.04967 [astro-ph.CO].

[64] E. Belgacem, S. Foffa, M. Maggiore, and T. Yang, Phys. Rev. D **101**, 063505 (2020), arXiv:1911.11497 [astro-ph.CO].

[65] Y. Li, Y. Hao, W. Cheng, and R. Rainer, (2019), arXiv:1904.05683 [physics.acc-ph].

[66] M. Bernardini, L. Mayer, D. Reed, and R. Feldmann, (2019), arXiv:1912.04299 [astro-ph.CO].

[67] A. Gómez-Valent and L. Amendola, in *15th Marcel Grossmann Meeting on Recent Developments in Theoretical and Experimental General Relativity, Astrophysics, and Relativistic Field Theories* (2019) arXiv:1905.04052 [astro-ph.CO].

[68] C. E. Rasmussen and C. K. I. Williams, *Gaussian Processes for Machine Learning* (MIT Press, 2006).

[69] T. Holsclaw, U. Alam, B. Sansó, H. Lee, K. Heitmann, S. Habib, and D. Higdon, Physical Review D **82**, 103502 (2010), arXiv:1009.5443 [astro-ph.CO].

[70] T. Holsclaw, U. Alam, B. Sansó, H. Lee, K. Heitmann, S. Habib, and D. Higdon, Physical Review Letters **105**, 241302 (2010), arXiv:1011.3079 [astro-ph.CO].

[71] T. Holsclaw, U. Alam, B. Sansó, H. Lee, K. Heitmann, S. Habib, and D. Higdon, Physical Review Letters **84**, 083501 (2011), arXiv:1104.2041 [astro-ph.CO].

[72] A. Shafieloo, A. G. Kim, and E. V. Linder, Physical Review D **85**, 123530 (2012), arXiv:1204.2272 [astro-ph.CO].

[73] M. Seikel, C. Clarkson, and M. Smith, Journal of Cosmology and Astroparticle Physics **6**, 036 (2012), arXiv:1204.2832.

[74] M.-J. Zhang and H. Li, European Physical Journal C **78**, 460 (2018), arXiv:1806.02981.

[75] M. Martinelli, N. B. Hogg, S. Peirone, M. Bruni, and D. Wands, Monthly Notices of the Royal Astronomical Society **488**, 3423 (2019), arXiv:1902.10694 [astro-ph.CO].

[76] F. Gerardi, M. Martinelli, and A. Silvestri, JCAP **1907**, 042 (2019), arXiv:1902.09423 [astro-ph.CO].

[77] N. B. Hogg, M. Bruni, R. Crittenden, M. Martinelli, and S. Peirone, Phys. Dark Univ. **29**, 100583 (2020), arXiv:2002.10449 [astro-ph.CO].

[78] M. Seikel and C. Clarkson, (2013), arXiv:1311.6678 [astro-ph.CO].

[79] S. Ambikasaran, D. Foreman-Mackey, L. Greengard, D. W. Hogg, and M. O'Neil, (2014).